Spatiotemporal distribution of Industrial Regions and Impact on LST in the case of Kocaeli, Turkey

Arzu Erener[1], Gulcan Sarp[2]

[1]*Department of Geomatics Engineering, Kocaeli University, 41380 Kocaeli, Turkey. e-mail: arzu.erener@kocaeli.edu.tr*
[2]*Department of Geography, Suleyman Demirel University, 32260 Isparta, Turkey. e-mail: gulcansarp@sdu.edu.tr*

ABSTRACT

Monitoring of urban sprawl especially the growth of industrial regions is an important task to maintain the balanced and sustainable development, to understand status of urban air pollution and ecosystems and to support urban planning. Additionally, it is also a fact that the increase in industrial areas negatively affects the global warming. Remote sensing images provide fast monitoring of multi-temporal spatial data and GIS (Geographic Information Systems) technologies has become an important tool for handling these spatial data. Satellite images are useful for land use mapping, change analysis, object determination, etc., as well as thermal bands provide an opportunity to determine the Land Surface Temperatures (LST).
Kocaeli is a high dense industrialized city with industrial institutions in various sectors as Petroleum Refineries, automotive, chemistry, textile, machine, food, paper, wood, tanning, coal, etc.. This paper aims to analyze the spatiotemporal change of industrial regions and determine the impact of these changes on surface temperature in industrial regions within 14 years period in the case of Kocaeli, Turkey. The change in industrial regions was determined with raster-based analysis by handling Landsat 7 ETM+ and Landsat 8 OLI satellite images belong to 2002 and 2016 years respectively. The remote sensing images were classified before the change analysis. As a result of the process, 35.15% increase in the field of the industry has been observed for 14 years. LST analysis was determined by handling Landsat 7 and Landsat 8 OLI satellite images belong to 2000 and 2016 years respectively. The spatiotemporal distribution of industrial region and its impact on surface temperature was investigated by analyzing the LST changes on industrial regions.

Spatiotemporal distribution of Industrial Regions and Impact on LST in the case of Kocaeli, Turkey

Arzu Erener, Gulcan Sarp

1. INTRODUCTION

Uncontrolled urbanization and especially the growth of industrial regions cause negative impacts on air pollution and ecosystem (Bhatta, 2010). Industrial production and power generation plants receive the first rank in carbon dioxide emissions (Atalık, 2007). In order to maintain balanced and sustainable development, prepare promising development and environmental plans and programs, the changes in land use/landcover should be monitored. Remote sensing images are one of the most important data sources about required up-to-date spatial information and GIS (Geographic Information Systems) technologies has become an important tool for handling these spatial data and in monitoring and managing rapid land use change. Additionally, the thermal bands of satellite images are widely used in dense urbanized areas, as well as in the identification of city heat islands (Kaya et al., 2012; Şekertekin et al., 2013; Sarp, 2016). Land-use/land-cover mapping and change detection in industrial and urban regions are adopted for different applications as: Sugumaran et al., 2002; Thomas et al., 2003; Shimoni et al., 2009; Lu et al., 2010; Akay and Sertel, 2016; Song et al., 2016. Most researchers have used multi-class Support Vector Machine (SVM) classification for land use detection of urban areas (Huang et al., 2002; Pal and Mather, 2003; Foody, and Mathur, 2004; Boyd, et al., 2006; Xie, 2006; Kavzoglu and Colkesen, 2009; Erener, 2013; Sarp et al., 2014; Wei et al., 2015) from high-resolution satellite images.

Global warming is the name given to the increase in average temperatures measured over the world all year round in land, sea, and air. LST derived from the thermal band is a significant parameter to determine the energy exchange between the surfaces of the earth (Shah et al., 2013; Orhan et al., 2014; Sarp, 2016). LST estimation by using the Thermal Infrared Region (TIR) were carried out by many researchers (Carnahan, and Larson, 1990; Hung et al., 2006; Rajasekar, and Weng, 2009; Falahatkar et al., 2011; Joshi, and Bhatt, B., 2012; Shah et al., 2013; Orhan and Ekici, 2015; Anbazhagan and Paramasivam, 2016; Sarp, 2016).

Kocaeli is one of the dense industrial provinces of Turkey and it is the Turkey's second largest industrial center after Istanbul. In this study it is aimed to monitor the spatiotemporal distribution of industrial regions using Landsat images in 14 years period in Kocaeli case. SVM has been selected as most promising classifier to be used within this study for the task of urban structure type pattern recognition within built-up areas. Additionally, it is aimed to analyze the impact of industrial region change on surface temperature using ETM+ and OLI thermal bands of Landsat satellite.

2. STUDY REGION

Kocaeli, is located to the east of the Marmara Sea The city lies between the 29°22'-31°22' eastern longitude and 40º31'-42º42' northern latitude and it carries a geopolitical importance as it is located in junction point of roads connecting Asia and Europe. Kocaeli is located on the border of Istanbul and it's on the D-100 and TEM highways therefore it became an industrial city after the 1980's due to it is ease of transportation. There are 12 districts in total and industrial areas in Kocaeli are generally located in the districts of Gebze, Çayırova, Dilovası, Kartepe, İzmit and Gölcük.

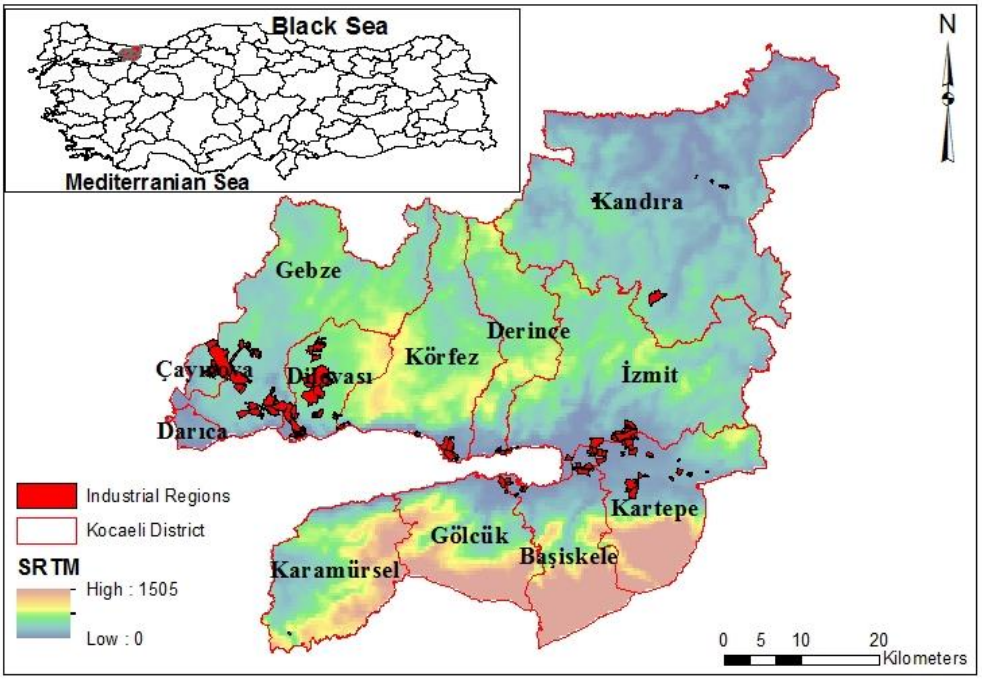

Figure 1. Location of the study area (a) Turkey's location (b) Kocaeli districts and distribution of industrial regions

3. DATASET AND METHODOLOGY

Landsat 7 ETM+ (enhanced thematic mapper plus) and Landsat 8 OLI images are available for the study area for the years of 18/07/2000, 07/02/2002, 22/07/2016 and 22/02/2016, respectively. The Landsat7 ETM+ for 07/02/2002 and Landsat 8 OLI for 22/02/2016 were used to obtain land use/landcover map of the region. The Landsat7 ETM+ for 18/07/2000 and Landsat 8 OLI for 22/07/2016 were used to obtain LST map of the region.
Atmospheric changes affect the radiometric resolution of the satellite image, at the same time substances such as clouds, snow, rainy weather can lead to errors when classifying and trying

to distinguish objects, and a separate class may be required for these substances. For this reason, it was noted to choose the satellite images that were belonging to the same month. The images were obtained from the http://earthexplorer.usgs.gov/ internet address freely. Detailed information for these images is listed in Table 1.

Table 1: Detailed information of Landsat ETM+ and Landsat 8 OLI images

Satellite	Year	Sensor	Spectral Range	Band #s	Scene Size	Pixel Resolution
L7 ETM+	07/02/2002 18/07/2000	multispectral	0.450-2.35 µm	1,2,3,4,5,7	185x185 km	30 m
L7 ETM+		thermal	10.40-12.50 µm	6.1, 6.2		60 m
L7 ETM+		panchromatic	0.52-0.90 µm	8		15 m
L8 OLI	22/02/2016 22/07/2016	multispectral	0.433-1.39	1,2,3,4,5,6,7,9	180x185	30 m
L8 OLI		thermal	10.6-12.5	10,11		100 m
L8 OLI		panchromatic	0.50-0.68	8		15 m

4. APPLICATION

Image preprocessing was carried out before obtaining land-use landcover maps. The clipping/subsetting process was carried out initially in the Kocaeli province in order to cover the industrial areas of Izmit Gulf. Then the 30 m resolution Landsat images were pansharpaned with pan band to obtain 15 m. spatial resolution images. The images were then enhanced to increase the determination of the features. After obtaining the landuse/landcover map by using SVM methods the accuracy was tested by using an error matrix. The LST was obtained using Landsat7 ETM+ for 2002 and Landsat 8 OLI for 2015. The Landsat 8 OLI for 2016 was not used for surface temperature due to radiance parameter error. The workflow of the study is presented in Figure 2.

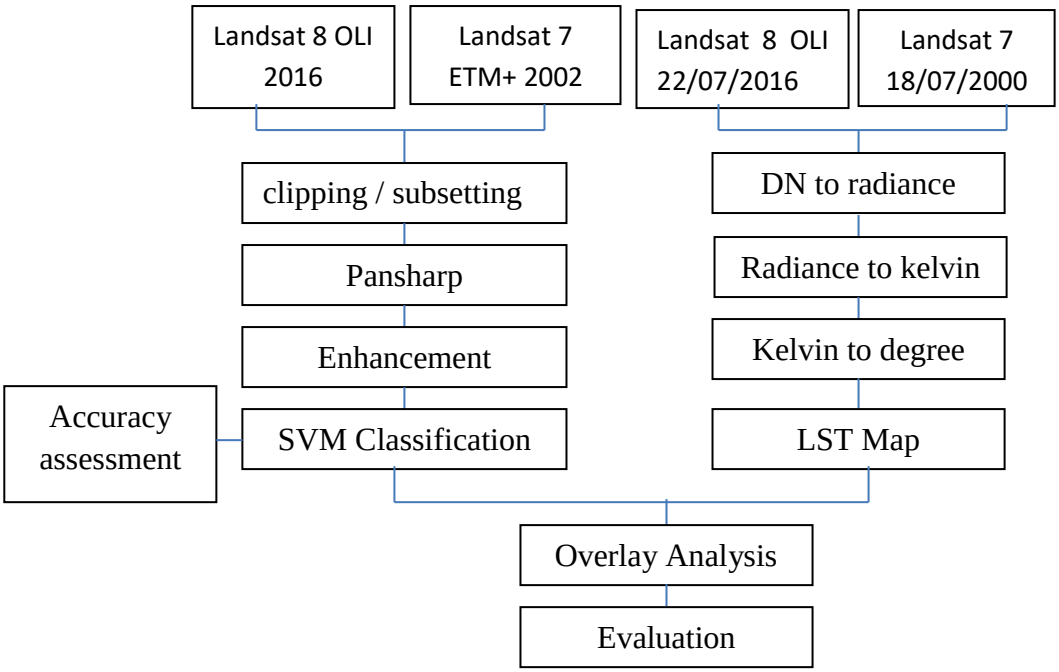

Figure 2. The workflow of the study

4.1. Spatiotemporal Industrial Region Analysis

In this study, SVM classification method was used to classify the images. SVMs and have been successfully used for data classification in the remote sensing (Boyd et al., 2006; Foody, 2008; Kavzoglu and Colkesen, 2009; Otukei and Blaschke, 2010; Erener, 2013) in various applications. SVM is a classifier derived from statistical learning theory and originally developed by Vapnik (1995). SVM method is divided into two depending on the data linearly separable and linear non-separable.

Classification with SVM for linearly separable data is intended to separate the samples of two classes, usually indicated by class labels of {-1, + 1}, with the help of a decision function obtained by training data. a hyperplane that can best distinguish the training data is obtained by using the decision function. In this method, two parallel lines (right and left) are formed at a certain distance of a hyperplane. The points lying on these lines are defined as the support vector.
In order to obtain the hyperplane for linearly separable data with two class, all samples in the data set must be provided with the following inequalities (Osuna and Freud, 1997).

$w.xi + b \geq +1$, $yi = +1$ (1)
$w.xi + b \leq -1$, $yi = -1$ (2)

where, x∈Rn is an n-dimensional space, y∈{+1,−1}is class label, w determines the direction of the discriminating plane, and b is the bias that determines the distance of the hyperplane from the origin.

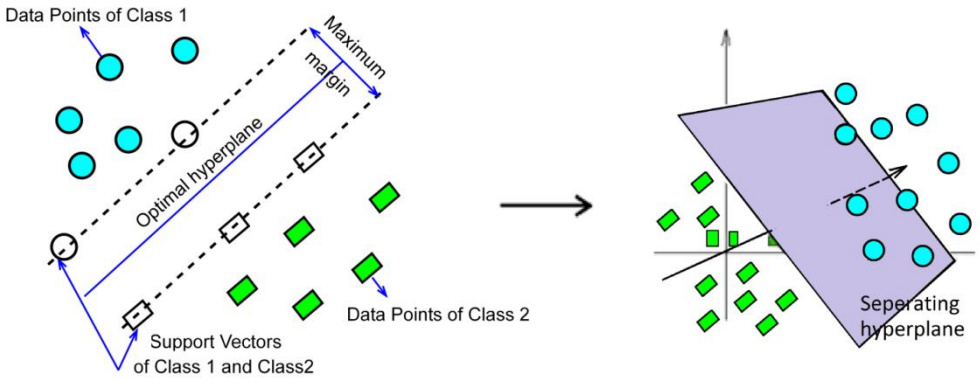

Figure 3. Linear support vector machine example (modified from Burges (1998)).

In remotely sensed images, the data is linearly non-separable. Kernel representations offer a solution in locating complex decision boundaries between classes. The SVM classifier provides four types of kernels: linear, polynomial, radial basis function (RBF), and sigmoid.

The mathematical representation of each kernel is given in below equations [3-6],

$$Linear: K(x_i, x_j) = x_i Tx_j \quad (3)$$

$$Polynomial: K(x_i, x_j) = (\gamma x_i Tx_j + r)d, \gamma > 0 \quad (4)$$

$$RBF: K(x_i, x_j) = \exp(-\gamma \| x_i - x_j \| 2), \gamma > 0 \quad (5)$$

$$Sigmoid: K(x_i, x_j) = \tanh(\gamma x_i Tx_j + \mathrm{r}) \quad (6)$$

where γ is the gamma term in the kernel function for all kernel types except linear, d is the polynomial degree term in the kernel function for the polynomial kernel, r is the bias term in the kernel function for the polynomial and sigmoid kernels, γ, d, and r are user depended parameters, as their correct definition significantly increases the accuracy of the SVM.

For SVM classification training areas were created by choosing polygons that contain training pixels representing the land covers. 8 land cover classes including water, industry, 3 different green regions, bare soil, urban and road were selected for training regions. The sigmoid kernel was used. The gamma in kernel function and penalty parameter was selected as 0.143 and 100 respectively. The result of the classification for 2002 and 2016 images is presented in Figure 4.

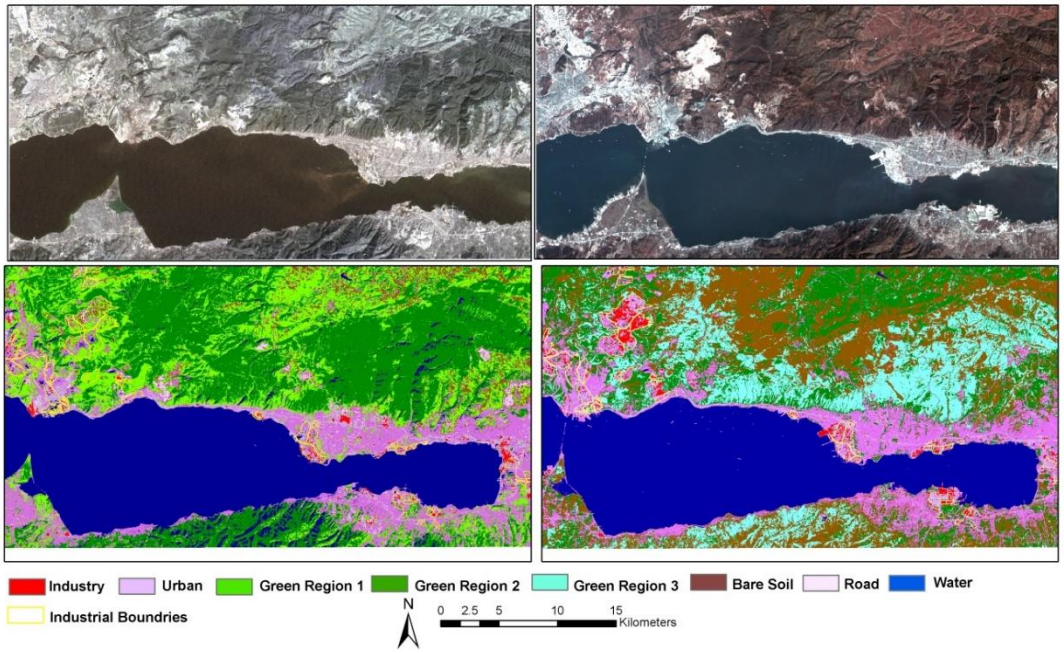

Figure 4. a. 2002 Landsat image b. 2016 Landsat image c. 2002 SVM classification map d. 2016 SVM classification map

For accuracy assessment purposes, selection of ground truth pixels was done by random sampling. Accuracy analysis was carried by comparing the classified pixels with ground truth pixels using a confusion matrix. The results were presented in terms of Kappa Coefficient and overall accuracy. According to the results, kappa coefficients and overall accuracy of 2002 is 99.87% and 0.9883, respectively. The kappa coefficients and overall accuracy of 2016 is %99.86 and 0.9856, respectively.

The classes other than the industry in 2002 and 2016 were combined into one class, reducing the number of classes to two (Figure 5). These images containing two classes were differentiated by change detection difference analysis. As a result of this process, 35.15% differences and increases in the field of industry have been observed for 14 years.

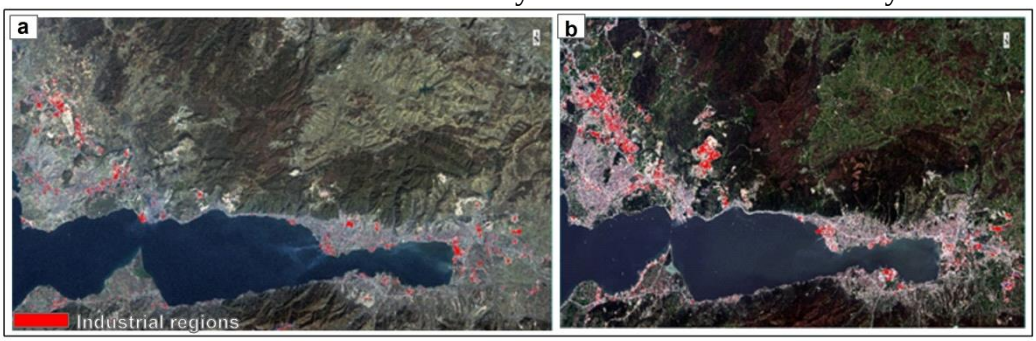

Figure 5. The industrial regions obtained by classification was overlaid with Landsat images a. 2002 industrial regions b. 2016 industrial regions

4.2. Land surface temperature (LST) estimation

In this study, LST was derived from a thermal band of the Landsat7 ETM+ satellite image and Landsat 8 OLI thermal bands for 2000 and 2016. The spectral radiance and quantized calibrated values in DNs from the relevant header file were obtained before calculating the radiance. The following formula was used to convert DNs to spectral radiance (Chander and Markham, 2003; USGS, 2013) (7).

$$L_\gamma = \frac{LMax_\lambda - LMin_\lambda}{QCalMax - QCalMin} \times (DN - QCalMin) + LMin_\lambda \quad (7)$$

Where; Lʎ is the spectral radiance at the sensors aperture in W/(m2* sr* μm); DN is the quantized calibrated pixel value, Lminʎ and Lmaxʎ are the minimum and maximum spectral radiance of thermal band respectively, QCalMin and QCalMax are the minimum and maximum quantized calibrated pixel value in DNs, respectively (NASA, 2011).

The spectral radiance (Lʎ) obtained by equation (7) is converted to satellite brightness temperature (Landsat project science office, 2002; USGS, 2013) by using the following conversion formula (8):

$$T = \frac{K_2}{\ln\left(\frac{K_1}{L_\lambda}\right)+1} \quad (8)$$

Where T is the effective at-satellite temperature in Kelvin (K), Lλ is the spectral radiance; K2 and K1 are the thermal band pre-launch calibration constants. For Landsat7 ETM+ band 6.1 image, K2 = 1282.71, and K1 = 666.09. For Landsat8 OLI band 10 images, K2 = 1321.08 and K1 = 774.89. The satellite temperature in Kelvin is then transformed to Celsius by using the equation (9):

$$T(C) = T - 273.15 \quad (9)$$

4.3.Relationship analysis between LST and industrial region

Industrial sprawl may cause negative impacts on global warming. Therefore, in this study, it is aimed to analyze the spatio-temporal variations in industrial regions. The LST maps obtained from 2000 and 2016 were presented in Figure 5. As it can be identified from the figure the maximum LST values for 2000 to 2015 were 50.14 and 49.74 respectively for the whole region. The technique of image differencing is employed to produce a radiant temperature change image after the surface radiant temperature of each year has been normalized (Fig. 5c). In order to investigate the relationship between the industrial regions and LST, the LST for 2000 and 2016 was overlaid with industrial region boundaries. Initially, 100 points were generated for industrial regions then the temperatures were resampled to the database from the 2000 and 2016 LSM maps. Then the temperature differences were obtained

and compared. The statistical parameters for 2000 and 2016 were displayed in Figure 7 and Table 2 for sample points around industrial regions.

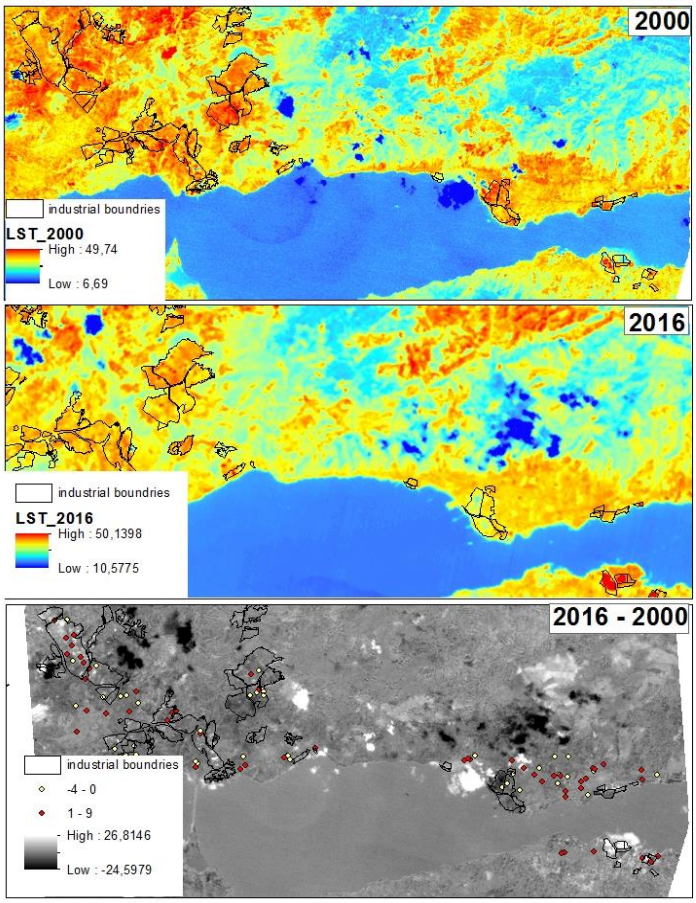

Figure 6. a. The LST for 2000 b. The LST for 2016 c. The LST difference map for 2000 to 2016

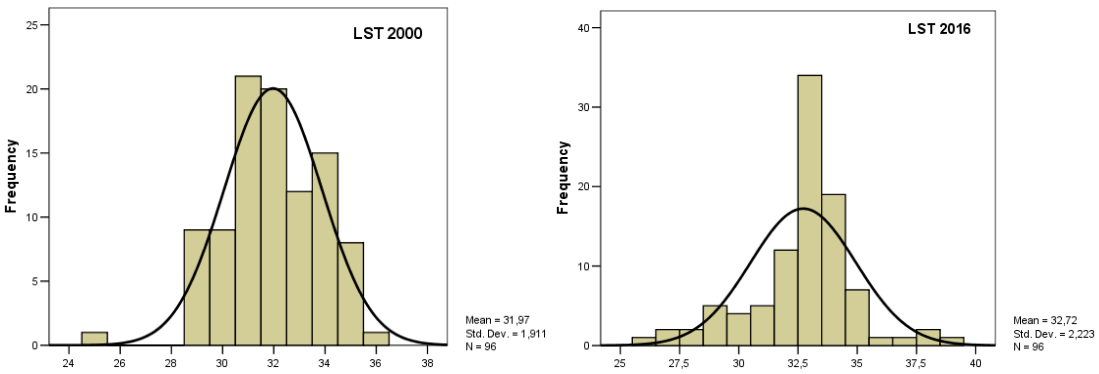

Figure 7. The frequency distribution for LST 2000 and LST 2016

Table 2. The statistics for sample points

Descriptive Statistics				
	Min.	Max.	Mean	Std. Dev.
LST 2000	25	36	31,97	1,911
LST 2016	26	39	32,72	2,223

5. CONCLUSION

In this study, an integrated approach of remote sensing and GIS was developed for evaluation of the spatiotemporal distribution of industrial region and its impact on surface temperature in Kocaeli city, Turkey. Temporal and spatial dynamics of industrial region distribution in relation to LST change was investigated using thermal infrared data of Landsat. The results indicate that 35.15% increase in the field of the industry has been observed for 14 years. The LST maps for 2000 and 2016 was obtained for the study region. The LST differences were analyzed on sample points for industrial regions. Its seen that the temperature increased 1 to 9 degrees at 60% of the sample points. The mean and maximum temperature increased 0.5 and 0.7 degrees respectively.

As a result, this study presents the effective use of remote sensing and GIS technologies on change and LST analysis. More efficient results will be obtained if the seasonal image temperatures are used instead of using the temperature differences from the satellite images taken in one day.

REFERENCES

Akay, S.S., Sertel, E., 2016. Urban Land Cover/Use Change Detection Using High Resolution Spot 5 and Spot 6 Images and Urban Atlas Nomenclature. The International Archives of the Photogrammetry. *Remote Sensing and Spatial Information Sciences* Volume XLI-B8, 2016 XXIII ISPRS Congress, 12–19 July 2016, Prague, Czech Republic, pp:789-796

Anbazhagan and Paramasivam, 2016. Statistical Correlation between Land Surface Temperature (LST) and Vegetation Index (NDVI) using Multi-Temporal Landsat TM Data. *Cloud Publications International Journal of Advanced Earth Science and Engineering,* 5(1) pp:333-346, Article ID Sci-409

Atalık, A., 2007. Küresel Isınma, Su Kaynakları ve Tarım Etkileşimi. *Ekoloji ve Çevre*, pp:1-9, http://www.zmo.org.tr/resimler/ekler/ce6d3c8830d27ec_ek.pdf, last visited on:26.02.2018

Bhatta, B., 2010. *Analysis of urban growth and sprawl from remote sensing data.* ISBN: 978-3-642-05298-9, Hardcover, p. 172

Boyd, D.S., Sanchez-Hernandez, C., Foody, G.M., 2006. Mapping a specific class for priority habitats monitoring from satellite sensor data. *International Journal of Remote Sensing* 27 (13), pp:2631–2644.

Carnahan, W.H. and Larson, R.C., 1990. An analysis of an urban heat sink. *Remote Sensing of Environment* 33, pp:65–71.

Erener, A., 2013. Classification Method, Spectral Diversity, Band Combination and Accuracy Assessment Evaluation for Urban Feature Detection. *International Journal of Applied Earth Observation and Geoinformation* DOI: 10.1016/j.jag.2011.12.008, 21(2013) pp:397–408

Falahatkar, S., Hosseini, S. M. and Soffianian, A. R., 2011. The relationship between land cover changes and spatialtemporal dynamics of land surface temperature. *Indian Journal of Science and Technology* 4 (2), pp:76-81.

Foody, G.M., Mathur, A., 2004. A relative evaluation of multiclass image classification,by support vector machines. *IEEE Transactions on Geoscience and Remote Sensing* 42, pp:1335–1343.

Huang, C., Davis, L. S., and Townsheng, J. R. G., 2002. An assessment of support vector machines for land cover classification. *International Journal of Remote Sensing* 23(4), pp:725-749.

Hung, T., Uchihama, D., Ochi, S. and Yasuoka, Y., 2006. Assessment with satellite data of the urban heat island effects in Asian mega cities. *International Journal of Applied Earth Observation and Geoinformation* 8, pp:34–48.

Joshi, J.P. and Bhatt, B., 2012. Estimating temporal land surface temperature using remote sensing: a study of vadodara urban area. *Gujarat, International Journal of Geology, Earth and Environmental Sciences* 2(1) pp:123-130.

Kavzoglu, T., Colkesen, I., 2009. A kernel functions analysis for support vector machines for land cover classification. *International Journal of Applied Earth Observation and Geoinformation* 11, pp:352–359.

Kaya, S., Basar, U.G., Karaca, M. and Seker, D.Z., 2012. Assessment of Urban Heat Islands Using Remotely Sensed Data. *Ekoloji* 21, 84, 107-113 (2012), pp:107-113

Lu, D., Hetrick, S., Moran, E., 2010. Land Cover Classification in a Complex Urban-Rural Landscape with QuickBird Imagery. *Photogrammetric Engineering & Remote Sensing* October 2010, 76 (10), pp:1159–1168.

Orhan, O., Ekercin, S., 2015. Konya Kapalı Havzasında Uzaktan Algılama Ve Cbs Teknolojileri Ile İklim Değişikliği Ve Kuraklık Analizi. *TUFUAB VIII. Teknik Sempozyumu* 21-23 Mayıs 2015 / Konya

Orhan, O., Ekercin, S., and Dadaser-Celik, F., "Use of Landsat Land Surface Temperature and Vegetation Indices for Monitoring Drought in the Salt Lake Basin Area, Turkey". The Scientific World Journal. 1-11, 2014.

Pal, M., and Mather, P. M., 2003. Support vector classifiers for land cover classification. *In Proceedings of Map India 2003 Conference*, New Delhi, India, January, 2003.

Rajasekar, U. and Weng, Q., 2009. Spatio-temporal modeling and analysis of urban heat islands by using Landsat TM and ETM+ imagery. *International Journal of Remote Sensing* 30, pp:3531-3548.

Sarp, G., 2016. Evaluation of Land Surface Temperature and Vegetation Relation Based on Landsat TM5 Data. *SCIREA Journal of Geosciences* 1(1) October 2016

Sarp, G., Erener, A., Duzgun, S. and Sahin, K., 2014. An approach for detection of buildings and changes in buildings using orthophotos and point clouds: A case study of Van Erciş earthquake. *European Journal of Remote Sensing* 47, pp:627-642 . doi: 10.5721/EuJRS20144735

Şekertekin, A., Kutoğlu, Ş. H. and Kaya, Ş., 2013. Uzaktan Algılama Verileri Yardımıyla Yer Yüzey Sıcaklığının Belirlenmesi. *TMMOB Harita ve Kadastro Mühendisleri Odası, 14. Türkiye Harita Bilimsel ve Teknik Kurultayı* 14-17 Mayıs 2013, Ankara

Shah, D.B., Pandya, M.R., Trivedi, H.J., and Jani, A.R., 2013. Estimating Minimum and Maximum Air Temperature Using MODIS Data Over Indo-Gangetic Plain. *Journal of Earth System Science Indian Academy of Sciences* 122 (6) 1593-1605

Song, X.-P., Sexton, J.O., Huang, C., Channan, S., Townshend, J.R., 2016. Characterizing the magnitude, timing and duration of urban growth from time series of Landsat-based estimates of impervious cover. *Remote Sensing of Environment* 175, pp:1-13.

Sugumaran, R., Zerr, D. and Prato, T., .2002. Improved urban landcover mapping using multitemporal IKONOS images for local government planning, *Canadian Journal of Remote Sensing* 28, pp:90–95.

Thomas, N., Hendrix, C. and Congalton, R. G., 2003. A comparison of urban mapping methods using high-resolution digital imagery. *Photogrammetric Engineering & Remote Sensing* 69(9) pp:963–972.

Wei, L., Miao, L., Xiuwan, C., 2015. Automatic Change Detection Of Urban Land-Cover Based On Svm Classification. *Geoscience and Remote Sensing Symposium (IGARSS)*, 2015 IEEE International, 10.1109/IGARSS.2015.7326111, pp:1686-1689.

Xie, C., 2006. Support Vector Machines for Land Use Change Modeling. *UCGE Reports Number 20243*, Master Thesis, CALGARY, ALBERTA, pp:1-128